FUSE: A Flow-based Mapping Between Shapes

Lorenzo Olearo University of Milano-Bicocca

Giulio Viganò University of Milano-Bicocca

Daniele Baieri University of Milano-Bicocca

lorenzo.olearo@unimib.it

giulio.vigano@unimib.it

daniele.baieri@unimib.it

Filippo Maggioli Pegaso University

filippo.maggioli@unipegaso.it

Simone Melzi University of Milano-Bicocca

simone.melzi@unimib.it

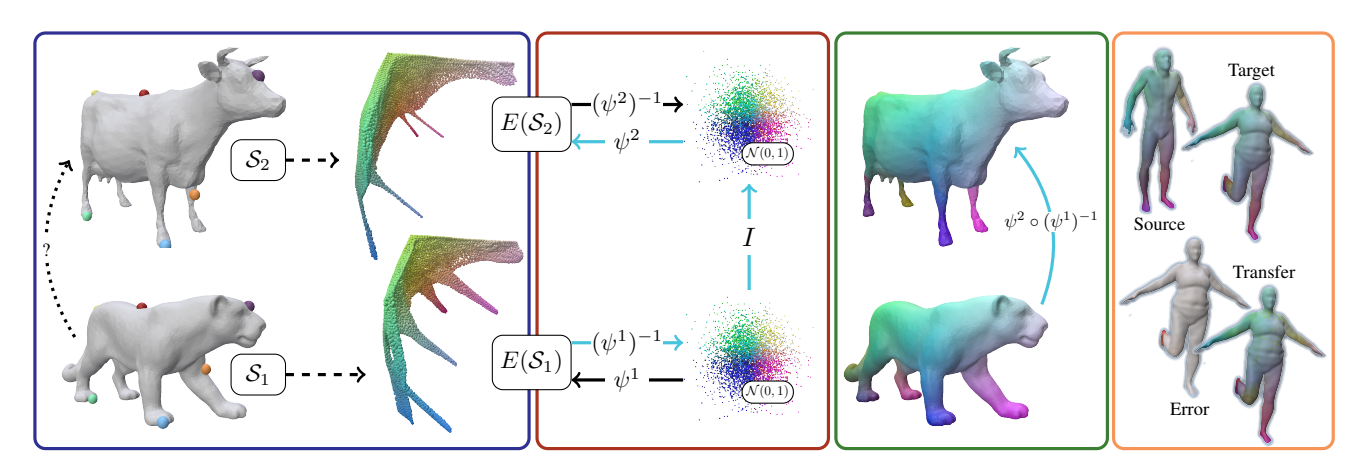


Figure 1. Our representation establishes a map between shapes S_1, S_2 by optimizing invertible flows (red box) between embedding distributions (blue box) and the unit Gaussian $\mathcal{N}(0,1)$. The composition of said flows (green box) is a continuous pointwise map between the surfaces, enabling shape matching and supporting various 3D representations, including neural signed distance fields (orange box).

Abstract

We introduce a novel neural representation for maps between 3D shapes based on flow-matching models, which is computationally efficient and supports cross-representation shape matching without large-scale training or data-driven procedures. 3D shapes are represented as the probability distribution induced by a continuous and invertible flow mapping from a fixed anchor distribution. Given a source and a target shape, the composition of the inverse flow (source to anchor) with the forward flow (anchor to target), we continuously map points between the two surfaces. By encoding the shapes with a pointwise task-tailored embedding, this construction provides an invertible and modalityagnostic representation of maps between shapes across point clouds, meshes, signed distance fields (SDFs), and volumetric data. The resulting representation consistently achieves high coverage and accuracy across diverse benchmarks and challenging settings in shape matching. Beyond shape matching, our framework shows promising results in

other tasks, including UV mapping and registration of raw point cloud scans of human bodies.

1. Introduction

Shape matching has long been recognized as a "key problem" in geometry processing: in fact, accurate correspondences between two shapes enable simple solutions for several downstream tasks (*e.g.*, pose transfer [47] or interpolation [15]). Most of the research in this field, following the common practices from 3D graphics industry, was built on the triangle mesh representation, which approximates a continuous 2-dimensional manifold embedded in \mathbb{R}^3 piecewise linearly with a collection of triangles connected by their common edges and vertices. However, recent progress in the fields of computer vision and deep learning has popularized novel ways of encoding 3D geometry, such as neural representations [35, 41]. These solutions offer several advantages compared to triangle meshes, but lack their large

suite of tools and algorithms for analysis and manipulation [56].

In this work, we address this challenge by introducing a novel representation for maps between a source and a target shape that can be applied over various geometric encodings. We namely refer to this representation as FUSE. Constructing a map with this representation requires only two components: i) the ability to sample points from the involved surfaces, and ii) a pointwise feature embedding designed for the target task. Once feature embeddings are computed for the sampled points on both source and target shapes, FUSE estimates an invertible flow from each embedding distribution to a shared anchor distribution, following Flow Matching framework [22]. FUSE then expresses the map between the two shapes as the composition of the inverse flow of the source (source \rightarrow anchor) and the forward flow of the target (anchor \rightarrow target). Note that, given the flows of any two shapes, the map is obtained in a "zero-shot" fashion, i.e., without any additional optimization or data.

In the context of shape matching, our representation introduces a probabilistic perspective on embedding alignment, where semantically similar features are encouraged to align through a shared probability distribution. Combined with the guarantee of mapping points directly into the target embedding space, our framework produces high-coverage and accurate correspondences that are relevant for different applications. We evaluate the proposed approach through a comprehensive experimental study, comparing it against several shape matching baselines, ranging from well-established axiomatic methods to recent data-driven approaches; FUSE shows high, if not the highest, accuracy on various benchmarks. Our contributions can be summarized as follows:

- We introduce FUSE, the first neural representation for 3D shape maps that naturally enables "zero-shot" correspondence between shapes expressed in different modalities (e.g., meshes, point clouds, and SDFs);
- We quantitatively show that FUSE achieves competitive or superior matching accuracy over state-of-the-art methods, particularly outperforming axiomatic approaches;
- We showcase the versatility of FUSE employing it as a backbone for downstream applications, including shape parametrization and point cloud deformation.

2. Related Work

2.1. Neural Shape Representations

Recent research in geometric deep learning and geometry processing popularized the practice of encoding 3D shapes in the weights of neural networks, which is referred to as neural shape representation. The early contributions in this field are due to Mescheder et al. [34] and Park et al. [41], followed by the introduction of NeRF [35], which led to

a vast effort to adapt neural shape representations to other tasks besides reconstruction. Examples of these adaptations are to shape deformation [1, 3, 37, 56], text-guided shape editing [25, 54] and generation [24, 43]. Recent contributions also introduced neural representations for 3D simulations [40] and computation of geometric operators over spherical neural surfaces [55].

The work of Koestler et al. [19] is closely related to ours, as they propose a method to represent functions continuously over surfaces in intrinsic space. Lastly, FUSE's architecture is inspired by Geometry Distributions [57], which proposes to represent geometry as a continuous map from a 3D Gaussian distribution to the surface with a denoising diffusion model [48]. However, by targeting the specific goal of representing maps between shapes, we build upon flow matching [22], and model flows directly over an intrinsic feature space, rather than standard Euclidean or extrinsic coordinates. These two choices together enable FUSE to represent mappings, as we prove by targeting the shape correspondence task.

2.2. Shape Matching

Shape correspondence is a fundamental task in geometry processing, with a wide range of approaches proposed over the years, which can largely be distinguished by how they represent the map between shapes and features [2, 7, 32, 49, 50]. Among these, the functional map framework [38] and its follow up works [8, 12, 27, 31, 33] have emerged as a dominant paradigm, where correspondences are represented as linear operators between functional spaces. These methods offer attractive properties such as smoothness and invariance to deformations, but the reliance on spectral bases limits their generalization to non-mesh representations [31] and in obtaining bijective maps [4, 30, 53].

Another class of approaches leverages optimal transport (OT) [11, 26, 45], where correspondences are represented via transport plans minimizing the cost of moving a distribution of features from one shape to another. While OT yields a permutation matrix that defines a global bijection between points, when both shapes are discretized with equal numbers of uniformly weighted samples, in real-world scenarios meshes often have different densities and feature representations. Alternatively, registration-based approaches directly optimize non-linear deformation fields in 3D [21, 44, 51]. The fields are often parameterized via deformation networks, or complex architechtures, achieving accurate alignments at the cost of solving computationally heavy optimization problems and depending on initialization or learned priors.

Hybrid approaches combine the strengths of the above formulations [8, 9, 17, 20, 39, 52], gaining in efficiency and robustness, but still relying on learned priors and struggling to generalize to other representations.

On a different perspective, FUSE offers a novel representation for maps. Based on flow matching [22], our method models a correspondence as a composition of continuous invertible flows between intrinsic feature spaces and a shared anchor distribution, inherently enforcing bijectivity and high-coverage in obtained maps, without learned priors or per-pair optimization in a pipeline naturally agnostic of the geometric representation.

3. Background

Shapes and Matching. A 3D shape \mathcal{S} is modeled as a compact two-dimensional manifold embedded in \mathbb{R}^3 . From a computational standpoint, single shapes may be represented in several ways: polygonal meshes, point clouds, signed distance functions and volumetric meshes are notable examples. In this work, we identify a shape \mathcal{S} as a continuous manifold from which we can sample unordered sets of points $\{x_i\}_{i=0}^n$, encoded by their 3D coordinates (i.e. $x_i \in \mathbb{R}^3$) independently from the adopted representations.

Given 3D shapes $S_1 = \{x_i\}_{i=1}^{n_1}$ and $S_2 = \{y_j\}_{j=1}^{n_2}$ with a common semantic, a point-to-point correspondence T_{12} maps each point x_i to its corresponding point y_j . Shape matching is the task of estimating such correspondence.

In the non-rigid scenario, estimating correspondences directly from 3D coordindates is challenging; thus, most methods describe the shapes via pointwise *features*, characterizing their semantics and geometry [13, 49, 50]. For each point $x_i \in \mathcal{S}_1$, we compute a vector of features $f_i \in \mathbb{R}^d$ that we can then store as a row in the *embedding matrix* $E_1 \in \mathbb{R}^{n_1 \times d}$ (same goes for \mathcal{S}_2). Ideally, one can solve for the correspondence directly by leveraging the similarity between these encodings [2]. In practice, more complex pipelines are required to align the features and retrieve the correspondence from their relations [38].

Flow Matching. Flow Matching (FM) [22, 23] is a framework for learning continuous-time probability paths $(p_t)_{t\in[0,1]}$ that transport a known source distribution p_0 (e.g., a Gaussian) to an unknown target p_1 (e.g., data samples). This is achieved by learning a velocity field $u_t(x)$ describing the instantaneous dynamics of the path, parameterized by a neural network. For each $x \in \mathbb{R}^d$, the velocity field induces a flow $\psi_t(x)$ as the solution of the ODE $\frac{d}{dt}\psi_t(x) = u_t(\psi_t(x))$ with initial condition $\psi_0(x) = x$. Crucially, the flow ψ_t is invertible and diffeomorphic: starting from any point sampled from p_1 , i.e., $x \sim p_1$, integrating the ODE backward yields a point $\psi_0^{-1}(x) \sim p_0$. The bidirectionality enables transport between distributions in both directions. Since u_t is generally intractable, Lipman et al. [22, 23] proposed Conditional Flow Matching (CFM), replacing u_t with a tractable conditional velocity

field $u_t(x_t \mid x_1)$, while preserving the same gradients:

$$\mathcal{L}_{CFM}(\theta) = \mathbb{E}_{t,x_1,x_t \sim p_t(\cdot \mid x_1)} \left[\| v_t^{\theta}(x_t) - u_t(x_t \mid x_1) \|^2 \right].$$
(1)

where \mathbb{E}_{t,x_1,x_0} represents the average over randomly sampled timesteps in [0,1] and over source and target samples $x_0 \sim p_0, x_1 \sim p_1$. A simple choice for the field is linear interpolation, $x_t = (1-t)x_0 + tx_1$ with $u_t = x_1 - x_0$. CFM training is thus simulation-free, although generating samples still requires integrating the learned ODE. In the reminder of the paper, we will refer to CFM simply as Flow Matching (FM).

4. FUSE

Given the overview presented in the previous section, we can now provide all the details of our novel representation FUSE which we outlined in Figure 1.

4.1. Flow Optimization

Given a pair of shapes $S_1 = \{x_i\}_{i=1}^{n_1}$, $S_2 = \{y_j\}_{j=1}^{n_2}$ and an embedding matrix $E_\ell \in \mathbb{R}^{n_\ell \times d}$ (with $\ell = 1$ or 2), we denote the resulting embedding distributions as $p^\ell = E_\ell$ (see blue box of Figure 1).

For each shape, we train an independent flow model that learns a continuous, invertible mapping $\psi^\ell\colon [0,1]\times \mathbb{R}^d\to \mathbb{R}^d$. This flow transports samples from a fixed, shared Gaussian $p_0=\mathcal{N}(0,1)^d$ (the anchor distribution) to the shape's embedding distribution p^ℓ , i.e. $\psi_1^l(x)\sim p^l$ given $x\sim p_0$. Each flow is parametrized by a neural network and trained via Conditional Flow Matching [22, 23] as we described earlier (see red box of Figure 1).

Each flow is trained independently on its shape, requiring only the ability to sample embeddings from the surface.

4.2. Bridging Representations

FUSE determines a map between shapes by composing their flows. Given the two trained flows ψ^1 and ψ^2 , we define the map from S_1 to S_2 as:

$$\Phi_{12} = \psi^2 \circ (\psi^1)^{-1} \tag{2}$$

This composition leverages the Gaussian distribution as a common anchor: we transport the embedding points from \mathcal{S}_1 back to the Gaussian via $(\psi^1)^{-1}$, then forward to \mathcal{S}_2 via ψ^2 as depicted in Figure 2. Our formulation offers several advantages:

- 1. Injection of invariances of the adopted embeddings in the output map;
- 2. For any pair of shapes represented by the respective flows from a common distribution, no additional training is required to obtain a map between them;
- 3. Representation invariance: creating a bridge with FUSE only requires sampling from the surface, which is possible and easy for most 3D representations.

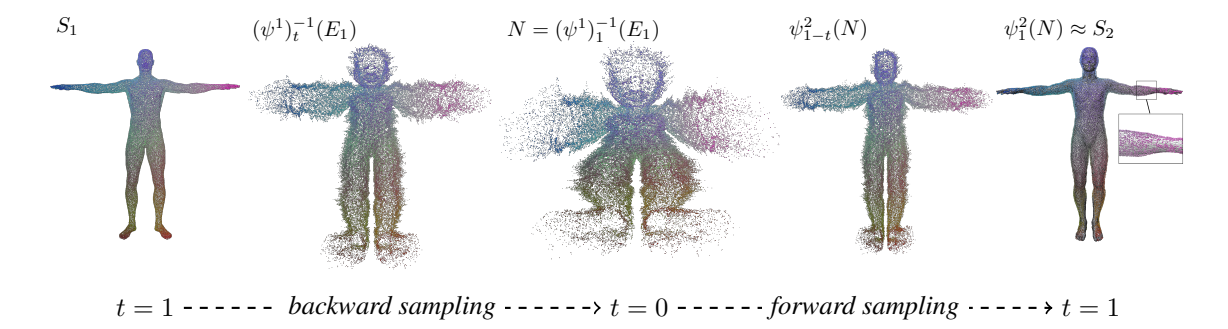


Figure 2. Visual example of the proposed pipeline. For visualization purpose, we select a pair for which we can solve for the correspondence using the 3D coordinates as features embedding. Estimated correspondence is encoded by the color (matched points have the same color).

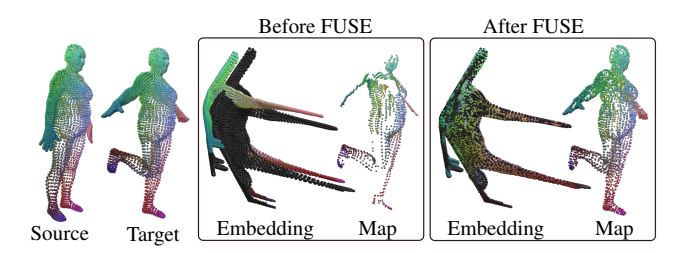


Figure 3. Effect of FUSE visualized on the first three coordinates of embedding and on the relative obtained map.

We can leverage this representation of maps between shapes to perform various tasks on the discrete geometry. For instance, if we want to retrieve the correspondence between points of two discretized shapes, we can perform the nearest search in the embedding space.

$$T_{12} = \text{NearestSearch}(\Phi_{12}(E_1), E_2) \tag{3}$$

Given the nature of the FM solutions and the selection of a shared Gaussian distribution as anchor, points with similar embeddings from different shapes are mapped to nearby regions in the anchor distribution (see green box of Figure 1). More importantly, by applying the flows, the embedding features will be aligned from a distributional point of view, and this alignment improves the accuracy of the estimated correspondence, as visualized in Figure 3.

4.3. Embedding Selection

The choice of embedding E is critical. First, to maintain the generalizability of FUSE to any representation of the 3D shape, all the representations must admit the computation of the selected embedding. Secondly, the embedding determines the properties of the FUSE map. For shape matching, we require encodings that capture metric and semantic information while being computable across different representations. Numerous embeddings to target shape matching between triangle meshes exist and leverage spectral signatures like WKS [2], neural architectures [46], or correspon-

dence supervision [8, 12]. While effective for matching, these methods depend on geometric priors (e.g., Laplacian eigenfunctions) or supervised data that are reliable only on meshes. In contrast, 3D coordinates are universally available but lack intrinsic geometric or semantic meaning, making them unsuitable for shape correspondence.

A possible solution, namely the geodesic feature embedding, is to represent each surface point as a vector of geodesic distances to a small set of landmarks L ($|L| \sim 5$). A small set of landmarks injects shape "semantics" into the algorithm without relying on other data priors.

The decision to use landmarks is consistent with the axiomatic shape matching methods employed in Functional Maps [38]. This geodesic feature embedding is compact, since each point is represented as a vector $\mathbb{R}^{|L|}_+$, and informative about the intrinsic geometry. Moreover, different algorithms have been developed to compute geodesic distances on triangle meshes, signed distance fields, and point clouds, such as Dijkstra's shortest path algorithm, the heat method [10] and fast marching [36].

However, geodesic embeddings are not naturally aligned across shapes from a distributional perspective. Feature distributions vary with sampling density and representation details, causing mismatches even between geometrically similar surfaces. With FUSE, the flow acts as a probabilistic alignment mechanism: by mapping geodesic features through the Gaussian prior, we obtain distributional alignment across shapes, as shown in Figure 3.

We perform quantitative and qualitative analysis of this behaviour in Table 1 and in Figure 4, where we compare the effect of FUSE with respect to the direct nearest search (KNN) on different embeddings in terms of the accuracy of the estimated correspondence and similarity of the distribution. Geodesic embeddings, initially less distributionally consistent, achieve levels of alignment comparable to learned features once transformed via the flow, confirming the role of flow matching as a probabilistic alignment mechanism across representations. If the features are nonalignable (xyz), then FUSE does not help. If the features are

Table 1. Comparison of embedding strategies (dimensionality reported aside) in terms of correspondence accuracy (\downarrow) and distributions similarity (\uparrow). Results computed over 45 isometric pairs.

Eb - 445	K	NN	FUSE (Ours)			
Embedding	Acc. ↓	Sim. ↑	Acc. ↓	Sim. ↑		
xyz (3)	0.020316	0.841044	0.030804	0.913107		
wks (10)	0.018615	0.904846	0.013043	0.971122		
geod (5)	0.003442	0.943582	0.002094	0.986980		
FMNet (30)	0.000062	0.990156	0.001158	0.988705		

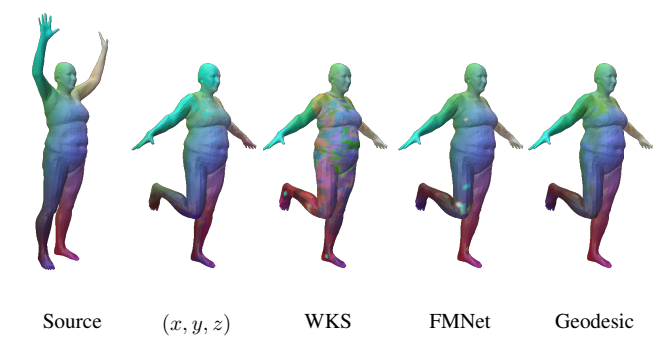


Figure 4. Correspondences obtained by FUSE with different embeddings. 3D coordinates (x,y,z) do not encode the semantic correspondence and cannot capture the non-rigid deformation. WKS does not solve intrinsic symmetries of the shape. With leaned embeddings (FMNet), our methods introduces small artifacts.

already aligned to a high degree (FMNet), the flow cannot improve them and may even slightly corrupt them. Otherwise, FUSE consistently improves the distributions similarity and the accuracy of the estimated correspondence.

4.4. Differences with Geomdist

The flow optimization described in Section 4.1 is closely related to GeomDist [57] (GD), which pioneered the idea of representing 3D shapes as probability distributions. However, we introduce two significant differences that are crucial for FUSE.

First, while GD uses denoising diffusion, FUSE employs Flow Matching which are two sides of the same coin [16], as both model generative dynamics from noise to data. However, a key distinction emerges when bridging multiple shapes. Flow matching defines an explicit interpolation between the Gaussian and the data distribution, guaranteeing that the inverse flow deterministically maps any shape back to the exact Gaussian. This ensures all shapes lie in a ideally shared latent space. GD, by contrast, only asymptotically approaches the Gaussian through large noise schedules, leading to deviations from the anchor space.

We quantify this effect in Table 2 evaluating shape pairs with geodesic embeddings using two criteria: (1) the JS and KL divergence between embedding distributions, and (2) the accuracy of nearest-neighbor correspondences in the

Table 2. DDIM vs FM in terms of probability divergence and in terms of obtained map accuracy (lower is better for all the metrics).

Metric	No Flow	DDIM (GD)	FM (Ours)
Euclidean Error	0.045	0.099	0.042
Geodesic Error	0.043	0.095	0.039
Euclidean Error (flow comp)	-	0.037	0.028
Geodesic Error (flow comp)	-	0.035	0.027
Mean KL Divergence	0.2528	0.3519	0.0375
Mean JS Divergence	0.1928	0.2128	0.0829

embedding space. We compute these metrics before and after inverting the flows using DDIM (GD) and FM (FUSE), and we also report accuracy after flow composition. The results show that FUSE achieves substantially lower divergence and higher correspondence accuracy, confirming that accurate anchoring to the Gaussian directly correlates with improved matching performance. GD's approximate inversion leads to larger deviations from the anchor and thus inferior map quality.

Second, GD represents only the coordinates of 3D shapes as distributions. While suitable for generation tasks, 3D coordinates lack the semantic and geometric information necessary for shape correspondence. For this reason, we propose for the first time to represent the more general embeddings as distributions.

5. Results

We extensively evaluate our representation, considering shape matching as the main task, but also presenting possible extensions of FUSE targeting other applications.

5.1. Non-Rigid Shape Matching

We first analyze the performance of FUSE against more standardized benchmark, considering pairs of meshes and point clouds. We then explore novel and more challenging scenarios by matching SDFs and inter-representation pairs.

Baselines. We evaluate FUSE against baselines ranging different paradigms. Methods using our same geodesic feature encoding include nearest neighbor search in the embedding space (KNN) and in the anchor distribution space (KNN-IN-GAUSS), OT (optimal transport with Sinkhorn relaxation [11]), Functional Maps with geodesic descriptors [38], and refined variants FM+ZO (ZoomOut [33]) and FM+NAM (Neural Adjoint Maps [52]). We also consider the original Functional Maps formulation with WKS [2], and the neural extrinsic Neural Deformation Pyramid (NDP) approach [21]. Finally, we use FUSE to initialize ZoomOut and NAM (FUSE +ZO and FUSE +NAM).

Table 3. Averaged results from all the considered datasets for our method and the other baseline solutions. For each column, the best result is highlighted in bold.

Method	FAUST (quasi-iso)			SMAL (non-iso)			SHREC20 (strong non-iso)			Kinect (point cloud)						
	Eucl. ↓	Geod. ↓	Dirich. ↓	Cov. ↑	Eucl. ↓	Geod. ↓	Dirich. ↓	Cov. ↑	Eucl. ↓	Geod. ↓	Dirich. ↓	Cov. ↑	Eucl. ↓	Geod. ↓	Dirich. ↓	Cov. ↑
KNN	0.0454	0.0434	0.0022	0.2452	0.0879	0.0836	0.0016	0.1364	0.1032	0.0731	0.0063	0.1481	0.1119	0.1095	0.0025	0.0995
OT [11]	0.0926	0.0856	0.0016	0.0890	0.0779	0.0741	0.0012	0.1129	0.1127	0.0879	0.0060	0.0992	0.1327	0.1273	0.0047	0.0748
FMAP [38]	0.0401	0.0400	0.0016	0.3236	0.0756	0.0744	0.0018	0.2162	0.1345	0.1754	0.0077	0.2086	0.0810	0.0779	0.0031	0.1683
FMAP-WKS [2]	0.0331	0.0334	0.0017	0.3759	0.0647	0.0623	0.0023	0.2585	0.1101	0.1131	0.0203	0.2402	0.0723	0.0718	0.0045	0.2211
ZO [33]	0.0207	0.0195	0.0009	0.6969	0.0625	0.0611	0.0065	0.4706	0.1232	0.1709	0.0099	0.3450	0.0706	0.0710	0.0062	0.4043
NAM [52]	0.0245	0.0240	0.0009	0.6323	0.0617	0.0589	0.0015	0.4694	0.1007	0.0771	0.0068	0.2866	0.0689	0.1118	0.0026	0.3494
NDP [21]	0.0702	0.0886	0.0020	0.4893	0.0555	0.0675	0.0010	0.4818	0.0725	0.0732	0.0014	0.4852	0.0457	0.0438	0.0012	0.4190
KNN-IN-GAUSS	0.0425	0.0390	0.0241	0.3483	0.0579	0.0542	0.0185	0.3708	0.0800	0.0635	0.0526	0.3477	0.0983	0.0925	0.0328	0.2459
Ours	0.0289	0.0274	0.0066	0.5320	0.0595	0.0576	0.0075	0.5156	0.0846	0.0692	0.0329	0.5213	0.0973	0.0914	0.0137	0.4931
Ours-ZO	0.0200	0.0189	0.0009	0.7127	0.0437	0.0413	0.0023	0.5361	0.1232	0.1709	0.0099	0.3705	0.0690	0.0662	0.0046	0.4173
Ours-NAM	0.0179	0.0168	0.0009	0.7027	0.0422	0.0388	0.0010	0.5520	0.0612	0.0450	0.0028	0.5252	0.0770	0.0702	0.0023	0.3904

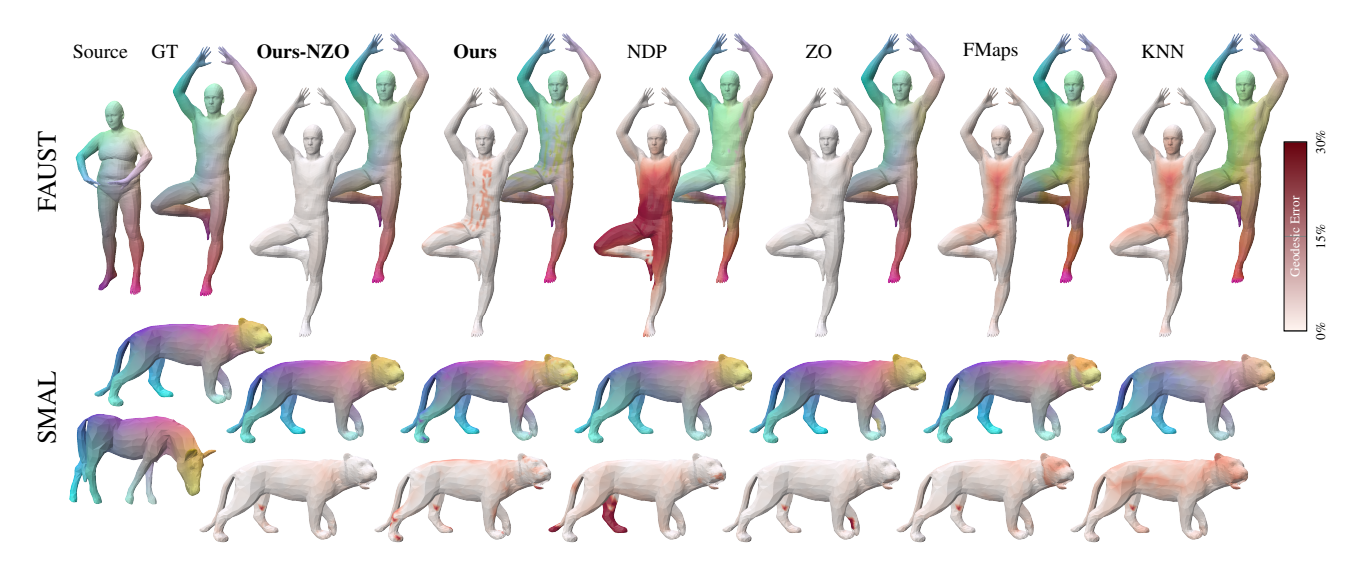


Figure 5. Qualitative evaluation: We report a pair of shapes with visualization of the p2p as transferred colormap and in terms of the geodesic error visualized via a hot-colormap. We note the lower but less smooth error of Ours compared to FMaps.

Datasets. We evaluate our method on well-established datasets for non-rigid shape matching:

- **FAUST** (meshes): a dataset of near-isometric human subjects in different poses [6] in a 1:1 correspondence.
- **SMAL** (meshes): composed of different classes of quadrupeds in varying poses with strongly non-isometric deformations [58]; we use the remeshed version of the dataset [8], where shapes have different discretizations.
- SHREC20 (meshes): 14 animal shapes including highly non-isometric pairs and shapes with missing parts [14]. No dense registration is provided, each pair is annotated with sparse set of landmarks; we consider all the pairs of the 5 test set and evaluate on the common landmarks between each shape pair.
- **KINECT** (point clouds): Kinect acquisitions of 15 human shapes interacting with objects from the BEHAVE dataset [5] with SMPL registrations, intoduced in [52].

We consider as landmarks sets of points taken at the protrusions of the shapes: 5 for the humans and 6 for the animals.

For SHREC20, we selected a subset of 6 landmarks that are common across all shape pairs.

Metrics. We evaluate the quality of correspondence using four metrics: two measures of accuracy, Euclidean (Eucl) and geodesic (Geod) distances [18], as well as Dirichlet energy [29] and coverage of the computed maps. Lower values are better for the first three metrics, while a higher value is better for Coverage. Quantitative results are reported in Table 3, qualitative in Figure 5.

Mesh correspondences. While FMaps-based methods tend to produce smoother maps, and thus to achieve a smaller Dirichlet energy, our method standouts in terms of both Euclidean and geodesics accuracy. Due to the nature of the flows, which are invertible by design, FUSE achieves better coverage of the target surface overall. The introduction of refinement strategies (*i.e.*, ZO and NAM) add pairwise optimization, further improving the base results that

we achieve with our pipeline and recovering smoothness. Notably, initializing the above mentioned methods with FUSE yields better results than using the standard FMaps initialization. This improvement can be even more appreciated by focusing on the results from the SHREC20 dataset, suggesting that our representation is more robust than simple feature embedding. Geodesic distances are particularly sensitive to deviations from isometry, and even though corresponding points can be associated with structurally similar distance distributions, the actual values may wildly vary.

We also observe that, in the more challenging scenario of non-isometric pairs, KNN-IN-GAUSS achieves slightly better accuracy than our approach, at the cost of a considerably higher Dirichlet energy. This suggests that the lack of smoothness in the maps produced by FUSE is imputable to the flow inversion from the surface to the anchor distribution, which is a non-smooth operation.

Point cloud correspondences. Point cloud matching presents a unique challenge: geodesic distances are unreliable on unstructured data, and uniform surface sampling is lost, since the surface information outside of the vertices is unknown. Consequently, FUSE's performance degrades. In contrast, NDP is extrinsic, and thus independent of feature quality, though it remains unreliable under strong non-rigid deformations (*e.g.*, FAUST). However, FUSE still outperforms non-refined geodesic methods (KNN, OT, FMAP), proving that the flow mechanism itself adds value.

5.2. Alternative Representations

Since FUSE only requires the ability to sample points from a surface and to compute single-to-all geodesic distances, it enables shape matching in a broader class of representations, such as Signed Distance Functions (SDFs), as well as inter-representation matching (see Figure 6).

SDFs shape matching. To our knowledge, no dataset exists for quantitatively evaluating matching between SDFs, so we introduce a new benchmark derived from FAUST. For each shape, we train a neural implicit model following [3], and for evaluation, we project the vertices of the original FAUST meshes onto their corresponding SDF surfaces, ensuring that accuracy is always measured on the original mesh geometry. We note that this implicit reconstruction may alter the topology of some shapes. To apply FUSE, we uniformly sample $\sim 10^5$ points from the zero level set and voxelize each SDF surface to compute geodesic distances via Dijkstra. As in Section 5.1, these geodesic embeddings are then used to train the flow models. Table 4 reports the results for all shapes whose SDFs preserve valid topology.

Inter-representation matching. We conduct experiments on shape pairs from different FAUST-like collections:

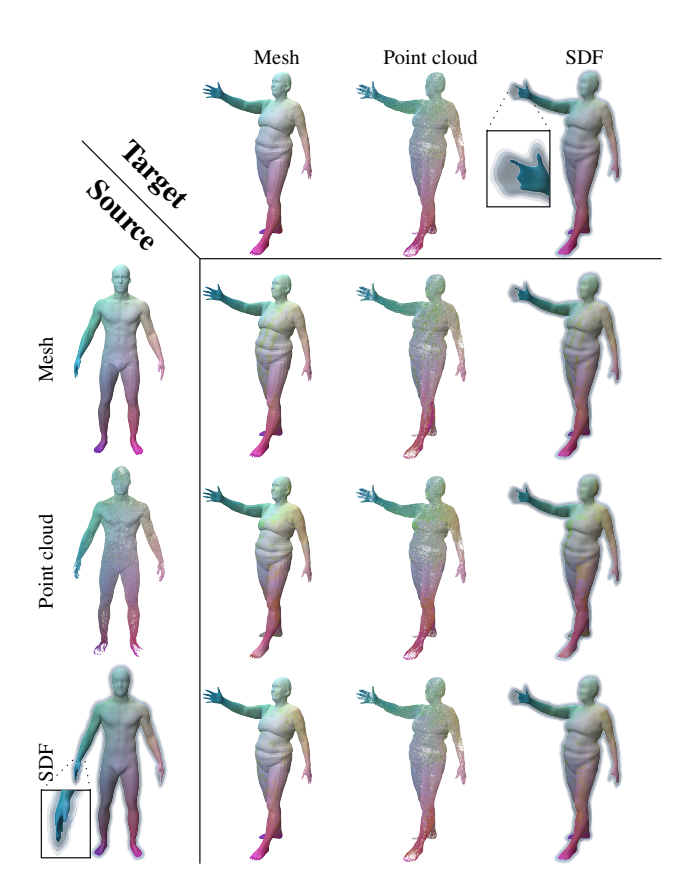


Figure 6. Coordinate transfer among different 3D representations enabled by FUSE.

Table 4. Quantitative evaluation of the SDF-based FAUST dataset without considering the topological error.

Method	Eucl. ↓	Geod. ↓	Dirich. ↓	Cov. ↑
KNN	0.0562	0.0569	0.0023	0.1744
knn-in-gauss	0.0472	0.0469	0.0175	0.2784
NDP	0.0525	0.0643	0.0016	0.5139
OT	0.0921	0.0881	0.0018	0.0936
Ours	0.0375	0.0385	0.0069	0.4653

from the original FAUST meshes, we extract the vertices to use as point clouds and compute SDFs as discussed in the previous paragraph. For each shape, gedesics are computed sticking to the constraints of the representation (*i.e.*, heat geodesics [10] on point clouds, Dijsktra on mesh or voxel grid). As mentioned in Section 5.1, FUSE inevitably struggles on matching tasks involving only point clouds, but achieves results comparable to mesh-to-mesh matching when at least one shape is represented as mesh or SDF. We provide an example of matching for all possible combinations of meshes, point clouds and SDFs in Figure 6. A deeper analysis is presented in the supplementary material.

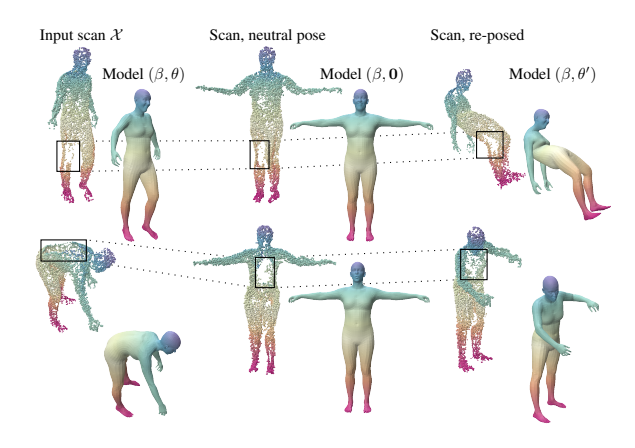


Figure 7. Results for human-scan fitting and skinning. Major defects in the input scans are preserved in the edited poses. We first optimize β and θ using FUSE correspondences, then re-pose the scan by applying point-wise offsets from the neutral pose.

5.3. Applications

FUSE allows modeling of 3D surfaces as probability distributions by means of surface sampling and to compute maps without an explicit optimization, effectively making it a "bridge" between distinct representations. We exploit this peculiar property to use FUSE as a backbone for various applications other than pure shape matching.

Human scans fitting and skinning. Given the scan of a human body, represented as a 3D point cloud S, we use FUSE to match it to a triangle mesh representing the neutral pose \mathcal{T} of a templated body model, which we obtain with SMPL-X [42]. By taking advantage of the correspondence, we can easily fit the body model's parameters to approximate S via minimization of the MSE between corresponding points. This procedure, whose results we show in the left column of Figure 7, yields style and pose vectors (β, θ) . If we compute the vertex displacement from the the output SMPL-X output for the optimized θ and the neutral pose \mathcal{T} , we can apply the same displacement to the corresponding points in S to obtain a point cloud in neutral pose. Given a second pose vector θ' , we can apply a similar process to obtain the scan in the second pose. Two example applications of our pipeline are depicted in Figure 7.

Mesh parametrization. Given a genus-zero surface S and a reference sphere Φ , we train flows from a Gaussian to each shape using 3D coordinates as embeddings. Composing these flows yields a bijection between S and Φ , allowing us to transfer the sphere's UV parametrization to the shape. Since FUSE maps may lack smoothness (see Section 5.1), the transferred UVs are used to supervise an MLP that predicts continuous UV coordinates, enforcing a smooth prior.

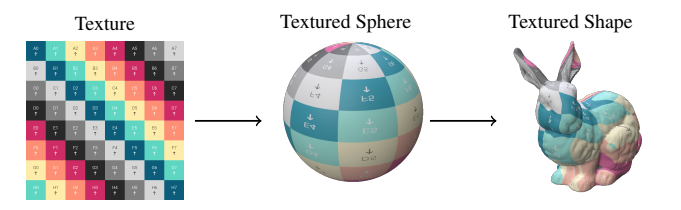


Figure 8. Illustration of our parametrization via texture mapping.

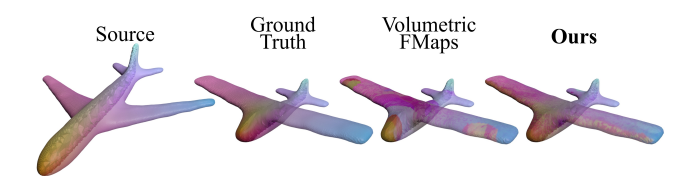


Figure 9. Qualitative comparison of Ours vs Volumetric Functional Maps on a pair of non isometric tetrahedral meshes.

Table 5. Volumetric correspondence by accuracy. and isometricity, details about the metric are in the supplementary material.

Mesh	T	Accuracy ↓				
	Isometry ↓	VolFmaps	Ours			
Cat	0.0561	0.0237	0.0422			
Octopus	0.0449	0.0151	0.0215			
Dino_skel	0.0851	0.0652	0.0426			
Airplane	0.2207	0.1273	0.0942			
Average	0.1017	0.0578	0.0501			

As the MLP operates in the embedding space, the procedure applies to any representation supported by FUSE. In this setting, 3D coordinates are sufficient, as no semantic consistency is required. In Figure 8 we show an example.

Volume matching. Our representation-agnostic formulation naturally extends to volumetric shapes, three-dimensional manifolds with well-defined geodesic distances, thus enabling targeting of volume-matching tasks. We apply our method to tetrahedral meshes and compare it to Volumetric Functional Maps [28]. Results from Table 5 and Figure 9 mirror our 2D analysis: comparable or improved matching accuracy, particularly in cases of strong non-isometry, where the functional approach struggle.

6. Conclusions and Limitations

We presented FUSE, a new representation for mapping between shapes inspired by the flow-matching framework. Matching pipelines built on FUSE offer a fresh perspective on shape correspondence, enforcing implicit bijectivity through continuous flows while maintaining, and in many cases improving, the quality of the final map. This allows us to obtain smooth, high-coverage correspondences that outperform traditional formulations.

Our method integrates naturally with diverse applications and learned settings, enabling joint feature extraction and universal geometric embeddings. Moreover, its probabilistic formulation offers an alternative to classical correspondence-based pipelines, suggesting new directions for flow-based alignment in future research.

References

- [1] Noam Aigerman, Kunal Gupta, Vladimir G. Kim, Siddhartha Chaudhuri, Jun Saito, and Thibault Groueix. Neural jacobian fields: learning intrinsic mappings of arbitrary meshes. *ACM Trans. Graph.*, 41(4), 2022. 2
- [2] Mathieu Aubry, Ulrich Schlickewei, and Daniel Cremers. The wave kernel signature: A quantum mechanical approach to shape analysis. In *Computer Vision Workshops (ICCV Workshops)*, 2011 IEEE International Conference on, pages 1626–1633. IEEE, 2011. 2, 3, 4, 5, 6
- [3] Daniele Baieri, Filippo Maggioli, Zorah Lähner, Simone Melzi, and Emanuele Rodolà. Implicit-arap: Efficient handle-guided deformation of high-resolution meshes and neural fields via local patch meshing, 2024. 2, 7
- [4] Lennart Bastian, Yizheng Xie, Nassir Navab, and Zorah Lähner. Hybrid functional maps for crease-aware nonisometric shape matching, 2024. 2
- [5] Bharat Lal Bhatnagar, Xianghui Xie, Ilya Petrov, Cristian Sminchisescu, Christian Theobalt, and Gerard Pons-Moll. Behave: Dataset and method for tracking human object interactions. In *IEEE Conference on Computer Vision and Pattern* Recognition (CVPR). IEEE, 2022. 6
- [6] Federica Bogo, Javier Romero, Matthew Loper, and Michael J Black. Faust: Dataset and evaluation for 3d mesh registration. In *Proceedings of the IEEE Conference* on Computer Vision and Pattern Recognition, pages 3794– 3801, 2014. 6
- [7] Davide Boscaini, Jonathan Masci, Simone Melzi, Michael M Bronstein, Umberto Castellani, and Pierre Vandergheynst. Learning class-specific descriptors for deformable shapes using localized spectral convolutional networks. *Computer Graphics Forum*, 34(5):13–23, 2015.
- [8] Dongliang Cao, Paul Roetzer, and Florian Bernard. Unsupervised learning of robust spectral shape matching. *ACM Trans. Graph.*, 42(4), 2023. 2, 4, 6
- [9] Dongliang Cao, Marvin Eisenberger, Nafie El Amrani, Daniel Cremers, and Florian Bernard. Spectral meets spatial: Harmonising 3d shape matching and interpolation, 2024. 2
- [10] Keenan Crane, Clarisse Weischedel, and Max Wardetzky. The heat method for distance computation. *Commun. ACM*, 60(11):90–99, 2017. 4, 7
- [11] Marco Cuturi. Sinkhorn distances: lightspeed computation of optimal transport. In *Proceedings of the 27th International Conference on Neural Information Processing Systems Volume 2*, page 2292–2300, Red Hook, NY, USA, 2013. Curran Associates Inc. 2, 5, 6
- [12] Nicolas Donati, Etienne Corman, and Maks Ovsjanikov. Deep orientation-aware functional maps: Tackling symmetry issues in shape matching. *CVPR*, 2022. 2, 4

- [13] Niladri Shekhar Dutt, Sanjeev Muralikrishnan, and Niloy J. Mitra. Diffusion 3d features (diff3f): Decorating untextured shapes with distilled semantic features. In *Proceedings of the IEEE/CVF Conference on Computer Vision and Pattern Recognition (CVPR)*, pages 4494–4504, 2024. 3
- [14] Roberto M. Dyke, Yu-Kun Lai, Paul L. Rosin, Stefano Zappalà, Seana Dykes, Daoliang Guo, Kun Li, Riccardo Marin, Simone Melzi, and Jingyu Yang. Shrec20: Shape correspondence with non-isometric deformations. *Computers & Graphics*, 92:28–43, 2020. 6
- [15] Marvin Eisenberger, David Novotny, Gael Kerchenbaum, Patrick Labatut, Natalia Neverova, Daniel Cremers, and Andrea Vedaldi. Neuromorph: Unsupervised shape interpolation and correspondence in one go, 2021. 1
- [16] Ruiqi Gao, Emiel Hoogeboom, Jonathan Heek, Valentin De Bortoli, Kevin Patrick Murphy, and Tim Salimans. Diffusion models and gaussian flow matching: Two sides of the same coin. In *The Fourth Blogpost Track at ICLR* 2025, 2025. 5
- [17] Puhua Jiang, Mingze Sun, and Ruqi Huang. Non-rigid shape registration via deep functional maps prior. In *Thirty-seventh Conference on Neural Information Processing Sys*tems, 2023. 2
- [18] Vladimir G Kim, Yaron Lipman, and Thomas Funkhouser. Blended intrinsic maps. In ACM Transactions on Graphics (TOG), page 79. ACM, 2011. 6
- [19] Lukas Koestler, Daniel Grittner, Michael Moeller, Daniel Cremers, and Zorah Lähner. Intrinsic neural fields: Learning functions on manifolds. In *Computer Vision – ECCV 2022*, pages 622–639, Cham, 2022. Springer Nature Switzerland.
- [20] Tung Le, Khai Nguyen, Shanlin Sun, Nhat Ho, and Xiaohui Xie. Integrating efficient optimal transport and functional maps for unsupervised shape correspondence learning. In 2024 IEEE/CVF Conference on Computer Vision and Pattern Recognition (CVPR), pages 23188–23198, 2024. 2
- [21] Yang Li and Tatsuya Harada. Non-rigid point cloud registration with neural deformation pyramid. In *Proceedings of the 36th International Conference on Neural Information Processing Systems*, Red Hook, NY, USA, 2022. Curran Associates Inc. 2, 5, 6
- [22] Yaron Lipman, Ricky TQ Chen, Heli Ben-Hamu, Maximilian Nickel, and Matt Le. Flow matching for generative modeling. *arXiv preprint arXiv:2210.02747*, 2022. 2, 3
- [23] Yaron Lipman, Marton Havasi, Peter Holderrieth, Neta Shaul, Matt Le, Brian Karrer, Ricky TQ Chen, David Lopez-Paz, Heli Ben-Hamu, and Itai Gat. Flow matching guide and code. arXiv preprint arXiv:2412.06264, 2024. 3
- [24] Ruoshi Liu, Rundi Wu, Basile Van Hoorick, Pavel Tok-makov, Sergey Zakharov, and Carl Vondrick. Zero-1-to-3: Zero-shot one image to 3d object. In *Proceedings of the IEEE/CVF International Conference on Computer Vision (ICCV)*, pages 9298–9309, 2023. 2
- [25] Steven Liu, Xiuming Zhang, Zhoutong Zhang, Richard Zhang, Jun-Yan Zhu, and Bryan Russell. Editing conditional radiance fields. In *Proceedings of the International Conference on Computer Vision (ICCV)*, 2021. 2
- [26] Yanbin Liu, Linchao Zhu, Makoto Yamada, and Yi Yang. Semantic correspondence as an optimal transport problem.

- In Proceedings of the IEEE/CVF Conference on Computer Vision and Pattern Recognition, pages 4463–4472, 2020. 2
- [27] Filippo Maggioli, Daniele Baieri, Emanuele Rodolà, and Simone Melzi. Rematching: Low-resolution representations for scalable shape correspondence. In *European Conference on Computer Vision*, pages 183–200. Springer, 2025. 2
- [28] Filippo Maggioli, Simone Melzi, and Marco Livesu. Volumetric functional maps, 2025. 8
- [29] Robin Magnet, Jing Ren, Olga Sorkine-Hornung, and Maks Ovsjanikov. Smooth non-rigid shape matching via effective dirichlet energy optimization. In 2022 International Conference on 3D Vision (3DV). IEEE, 2022. 6
- [30] Riccardo Marin, Simone Melzi, Pietro Musoni, Filippo Bardon, Marco Tarini, and Umberto Castellani. CMH: Coordinates Manifold Harmonics for Functional Remeshing. In *Eurographics Workshop on 3D Object Retrieval*. The Eurographics Association, 2019.
- [31] Riccardo Marin, Marie-Julie Rakotosaona, Simone Melzi, and Maks Ovsjanikov. Correspondence learning via linearlyinvariant embedding. In *Proceedings of the 34th Interna*tional Conference on Neural Information Processing Systems, Red Hook, NY, USA, 2020. Curran Associates Inc. 2
- [32] Simone Melzi, Maks Ovsjanikov, Giorgio Roffo, Marco Cristani, and Umberto Castellani. Discrete time evolution process descriptor for shape analysis and matching. ACM Transactions on Graphics (TOG), 37(1):4:1–4:18, 2018. 2
- [33] Simone Melzi, Jing Ren, Emanuele Rodolà, Abhishek Sharma, Peter Wonka, and Maks Ovsjanikov. Zoomout: Spectral upsampling for efficient shape correspondence. *ACM Transactions on Graphics (TOG)*, 38(6):155:1–155:14, 2019. 2, 5, 6
- [34] Lars Mescheder, Michael Oechsle, Michael Niemeyer, Sebastian Nowozin, and Andreas Geiger. Occupancy networks: Learning 3d reconstruction in function space. In *Proceedings IEEE Conf. on Computer Vision and Pattern Recognition (CVPR)*, 2019. 2
- [35] Ben Mildenhall, Pratul P. Srinivasan, Matthew Tancik, Jonathan T. Barron, Ravi Ramamoorthi, and Ren Ng. Nerf: Representing scenes as neural radiance fields for view synthesis. In ECCV, 2020. 1, 2
- [36] Facundo Mémoli and Guillermo Sapiro. Fast computation of weighted distance functions and geodesics on implicit hypersurfaces. *Journal of Computational Physics*, 173(2):730– 764, 2001. 4
- [37] Tiago Novello, Vinícius da Silva, Guilherme Schardong, Luiz Schirmer, Hélio Lopes, and Luiz Velho. Neural implicit surface evolution. In *Proceedings of the IEEE/CVF International Conference on Computer Vision (ICCV)*, pages 14279–14289, 2023. 2
- [38] Maks Ovsjanikov, Mirela Ben-Chen, Justin Solomon, Adrian Butscher, and Leonidas Guibas. Functional maps: a flexible representation of maps between shapes. *ACM Transactions on Graphics (TOG)*, 31(4):30:1–30:11, 2012. 2, 3, 4, 5, 6
- [39] G. Pai, J. Ren, S. Melzi, P. Wonka, and M. Ovsjanikov. Fast sinkhorn filters: Using matrix scaling for non-rigid shape correspondence with functional maps. In 2021 IEEE/CVF Conference on Computer Vision and Pattern Recognition

- (CVPR), pages 384–393, Los Alamitos, CA, USA, 2021. IEEE Computer Society. 2
- [40] Shaowu Pan, Steven L. Brunton, and J. Nathan Kutz. Neural implicit flow: a mesh-agnostic dimensionality reduction paradigm of spatio-temporal data. *J. Mach. Learn. Res.*, 24 (1), 2023. 2
- [41] Jeong Joon Park, Peter Florence, Julian Straub, Richard Newcombe, and Steven Lovegrove. Deepsdf: Learning continuous signed distance functions for shape representation. In *Proceedings of the IEEE/CVF conference on computer vision and pattern recognition*, pages 165–174, 2019. 1, 2
- [42] Georgios Pavlakos, Vasileios Choutas, Nima Ghorbani, Timo Bolkart, Ahmed A. A. Osman, Dimitrios Tzionas, and Michael J. Black. Expressive body capture: 3D hands, face, and body from a single image. In *Proceedings IEEE Conf.* on Computer Vision and Pattern Recognition (CVPR), pages 10975–10985, 2019. 8
- [43] Ben Poole, Ajay Jain, Jonathan T. Barron, and Ben Mildenhall. Dreamfusion: Text-to-3d using 2d diffusion. In The Eleventh International Conference on Learning Representations, 2023. 2
- [44] Alessandro Raganato, Gabriella Pasi, and Simone Melzi. Attention And Positional Encoding Are (Almost) All You Need For Shape Matching. Computer Graphics Forum, 2023. 2
- [45] Mahdi Saleh, Shun-Cheng Wu, Luca Cosmo, Nassir Navab, Benjamin Busam, and Federico Tombari. Bending graphs: Hierarchical shape matching using gated optimal transport, 2022. 2
- [46] Nicholas Sharp, Souhaib Attaiki, Keenan Crane, and Maks Ovsjanikov. Diffusionnet: Discretization agnostic learning on surfaces. ACM Trans. Graph., 41(3), 2022. 4
- [47] Chaoyue Song, Jiacheng Wei, Ruibo Li, Fayao Liu, and Guosheng Lin. 3d pose transfer with correspondence learning and mesh refinement, 2021. 1
- [48] Jiaming Song, Chenlin Meng, and Stefano Ermon. Denoising diffusion implicit models, 2022.
- [49] Jian Sun, Maks Ovsjanikov, and Leonidas Guibas. A concise and provably informative multi-scale signature based on heat diffusion. *Computer graphics forum*, 28(5):1383–1392, 2009. 2, 3
- [50] Federico Tombari, Samuele Salti, and Luigi Di Stefano. Unique signatures of histograms for local surface description. In *Proc. ECCV*, pages 356–369. Springer, 2010. 2, 3
- [51] Giovanni Trappolini, Luca Cosmo, Luca Moschella, Riccardo Marin, Simone Melzi, and Emanuele Rodolà. Shape registration in the time of transformers. *Advances in Neural Information Processing Systems*, 34:5731–5744, 2021. 2
- [52] Giulio Viganò, Maks Ovsjanikov, and Simone Melzi. Nam: Neural adjoint maps for refining shape correspondences. ACM Trans. Graph., 44(4), 2025. 2, 5, 6
- [53] Giulio Viganò and Simone Melzi. Bijective upsampling and learned embedding for point clouds correspondences. *Computers and Graphics*, 122:103985, 2024. 2
- [54] Can Wang, Menglei Chai, Mingming He, Dongdong Chen, and Jing Liao. Clip-nerf: Text-and-image driven manipulation of neural radiance fields. 2022 IEEE/CVF Conference on Computer Vision and Pattern Recognition (CVPR), pages 3825–3834, 2021. 2

- [55] Romy Williamson and Niloy J. Mitra. Neural geometry processing via spherical neural surfaces. *Computer Graphics Forum*, 44(2):e70021, 2025. 2
- [56] Guandao Yang, Serge Belongie, Bharath Hariharan, and Vladlen Koltun. Geometry processing with neural fields. In *Thirty-Fifth Conference on Neural Information Processing Systems*, 2021. 2
- [57] Biao Zhang, Jing Ren, and Peter Wonka. Geometry distributions, 2024. 2, 5
- [58] Silvia Zuffi, Angjoo Kanazawa, David Jacobs, and Michael J. Black. 3D menagerie: Modeling the 3D shape and pose of animals. In *Proceedings IEEE Conference on Computer Vision and Pattern Recognition (CVPR) 2017*, pages 5524–5532, Piscataway, NJ, USA, 2017. IEEE. 6